Journal of Crystal Growth 32 (1976) 335–349

FILAMENTOUS GROWTH OF CARBON THROUGH BENZENE DECOMPOSITION

A. OBERLIN and M. ENDO *
Laboratoire Marcel Mathieu, Faculté des Sciences, CNRS, ER 131, 45045 Orléans-La-Source, France

and

T. KOYAMA
Shinshu University, Faculty of Engineering, 500 Wakasato Nagano City, Japan

Received 19 September 1975

Carbon fibres have been prepared by pyrolysing a mixture of benzene and hydrogen at about 1100°C. They have been studied by high resolution electron microscopy. These fibres have various external shapes and contain a hollow tube with a diameter ranging from 20 to more than 500 Å along the fibre axis. They consist of turbostratic stacks of carbon layers, parallel to the fibre axis, and arranged in concentric sheets like the "annual ring structure of a tree". These fibres have two textures resulting from different growth processes; core regions, made of long, straight and parallel carbon layers, are primarily formed by catalytic effect; the external regions correspond to a pyrolytic deposit occurring during the secondary thickening growth process. Very small cementite crystals, typically about 100 Å in diameter, have been identified by dark-field techniques at the tip of the central tube of each fibre. A model of fibre growth related to a surface diffusion of carbon species on the catalyst particle has been established.

1. Introduction

Filamentous growth of carbon has been studied by many authors [1–7]. The fibres grow from various substrates heat-treated from 250°C to 2500°C in atmospheres containing either carbon monoxide or hydrocarbon gases. Some low temperature forms (below 1500°C) often are improperly called whiskers because they are not crystallized and have no epitaxial relation with the substrate from which they grow. Some of these filaments have been found to be hollow tubes with the carbon layers parallel to the fibre axis and more or less bent cylindrically so that their *c* axis should be perpendicular to the filament axis.

One of the authors [8,9] has reported that a great number of carbon fibres were obtained by pyrolysing a mixture of benzene and hydrogen at about 1100°C. The fibre lengths were up to 25 cm and their diameters less than several hundred micrometres. The SEM studies have shown that these fibres consist of concentric sheets of carbon, set around the fibre axis, as the annual rings of a tree. Also, like in a tree the fibres may be divided into two or more branches. Evidence has been given in another paper [10] that the growth process begins with the formation of thin filaments (primary process) which are progressively thickened by a secondary processing consisting in a deposit of carbon on the primary filament. In this pyrolytic thickening process the diameter increases as pyrolysing temperature and time increase. However, it is impossible to obtain the two stages separately because they are statistically concomitant, though successive for a given part of the fibre. It has also been shown [11] that the final fibres are graphitizable when heat-treated up to 2900°C.

The present paper mainly deals with the texture both of the primary filaments and of the subsequent deposit, which have been studied by high resolution electron microscopy (using a Philips EM 300). In order to decrease the thickness of the fibres the concentration of benzene was lowered and the growing time

* Permanent address. Shinshu University, Faculty of Engineering, 500 Wakasato Nagano City, Japan.

shortened, so that the diameters of the fibres have been restricted to less than 8000 Å; then most of them are thin enough for TEM studies. The fibres thus were either directly deposited on grids covered with a thin supporting carbon film or transversally thin sectioned by ultra-microtomy. Combined techniques were used such as selected area electron diffraction (SAD), bright- and dark-field especially developed in our laboratory [12,13] as well as lattice-imaging [14].

2. Experimental

2.1. Main part of the fibres

The external shape of the fibres greatly varies as shown in fig. 1. Many of them are bead-like, each bead being spindle-shaped, others are cylindrical with or without more or less constricted regions. All of them contain a tube running parallel to the axis (see arrows

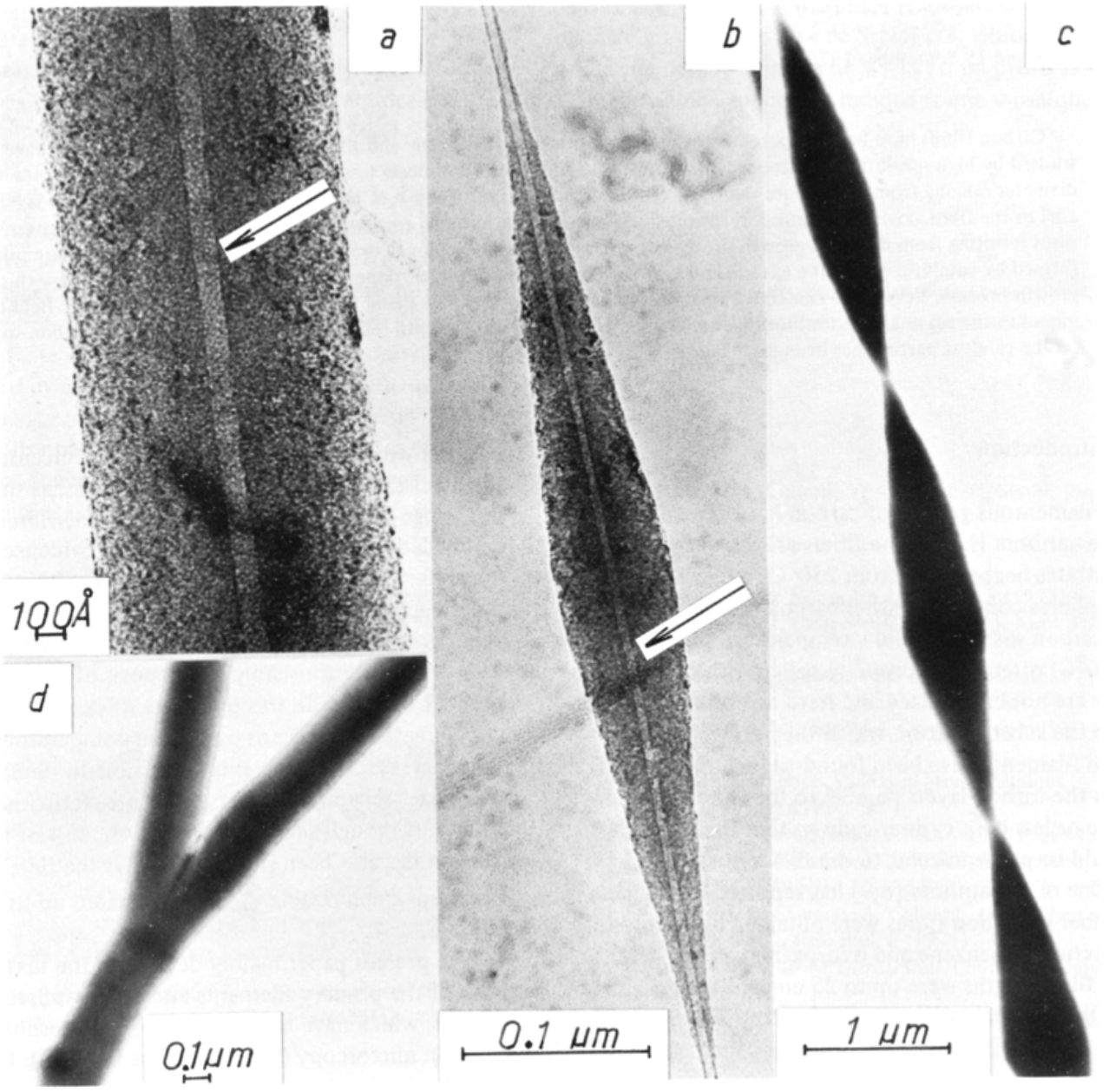

Fig. 1. Bright-field pictures of carbon fibres: (a) cylindrical, (b) spindle-shaped, (c) constricted, (d) branched

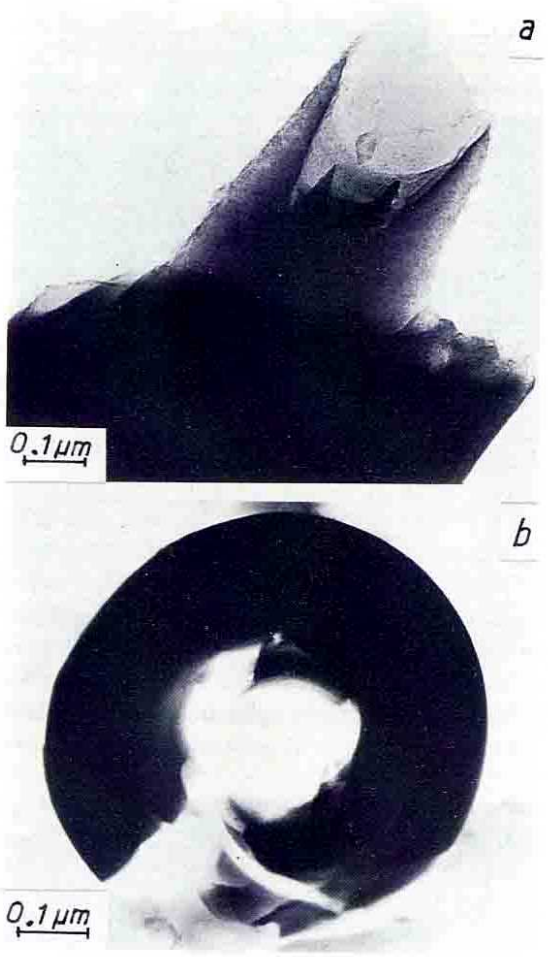

Fig. 2. (a) Fractured fibre with protruding cylindrical edge (b) transverse section (the core fell under the knife).

in fig. 1), the diameter of which widely varies from about 20 Å to more than 500 Å. The width of these tubes is not always constant over the whole length of a given fibre. The fibres are formed like a tree by concentric rings, the mutual adhesion of which is often very low. This is shown as an example in figs. 2a and 2b. In fig. 2a, the fragment of broken filament shows a large sheet peeled off while the core remains intact. In fig. 2b (transverse thin section), a part of the "annual ring structure of the tree" can only be seen; the central core fell under the microtome knife action. The core of the fibre seems to exhibit a higher strength than the outer part as shown in fig. 3.

The SAD patterns correspond to a turbostratic structure since they do not show any *hk.l* reflections characteristic of the three-dimentional crystalline order. They are representative patterns of a fibre in which all the carbon layers are roughly parallel to the fibre axis but in which the *a* axes are at random. The reciprocal space of such a fibre consists in 00.*l* nodes aligned along a direction perpendicular to the fibre axis (along equatorial line). The *hk* lines of turbostratic stacks generate concentric *hk* cylinders which turn around the fibre axis. If the reciprocal space is sectioned by a plane, a series of diffusion *hk* zones is obtained. They are limited internally by a circle centred on the 00.0 origin and externally by two straight lines parallel to the equatorial line. In fig. 4 the planar section schematically represents the case of a 10 cylinder only.

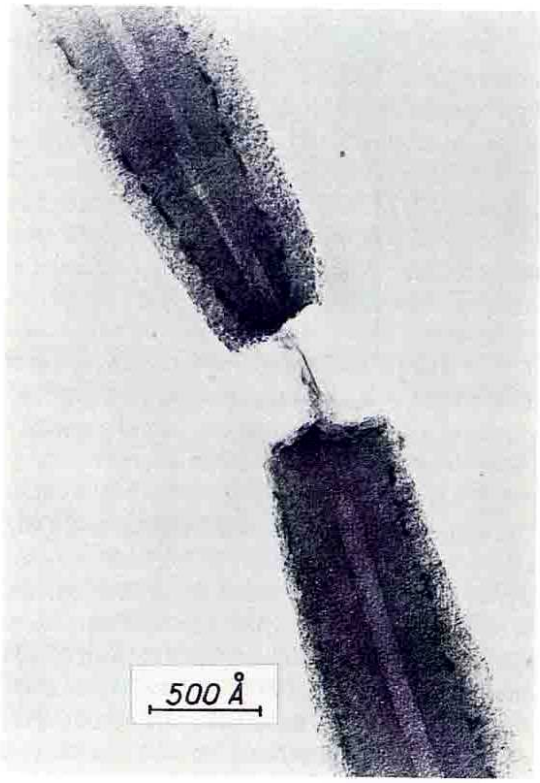

Fig. 3. Broken part of a fibre with remaining core.

When the SAD patterns are properly oriented in respect to the fibre axis (fig. 5a), they correspond to the above model. However, the 00.*l* reflections spread into arcs from 20 to 30°. The existing misorientation of aromatic layers is thus shown to be equal to this value.

These patterns cannot be used to determine wheth-

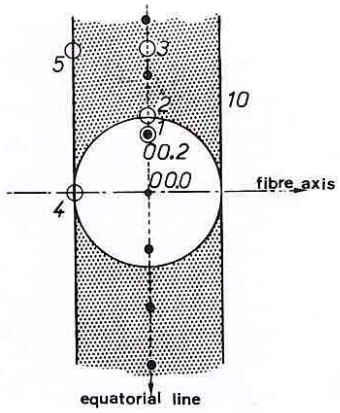

Fig. 4. Section of a part of the reciprocal space of a fibre showing various positions of the objective aperture

er the texture of the fibre is cylindrical or not. Only the dark-field technique allows such a determination. However additional information about the elementary stacks can be given by SAD patterns. First, the occurrence of high-order 00.*l* reflections (up to 00.8) indicates a good parallelism of the carbon layers as well as the absence of distorsions. Secondly, the sharpness of the 00.2 reflections depends on the diameter of the fibres. The thickest ones (fig. 5a) lead to more diffuse reflections than the thinnest ones (fig. 5b). Consequently, the number of layers per stack is smaller in

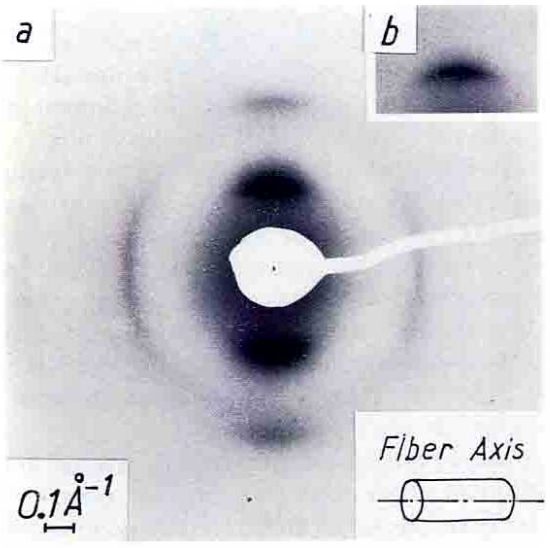

Fig. 5. Selected area electron diffraction pattern of a cylindrical fibre; the axis is perpendicular to the incident beam: (a) thick fibre, (b) thin fibre (detail of 00.2 reflection).

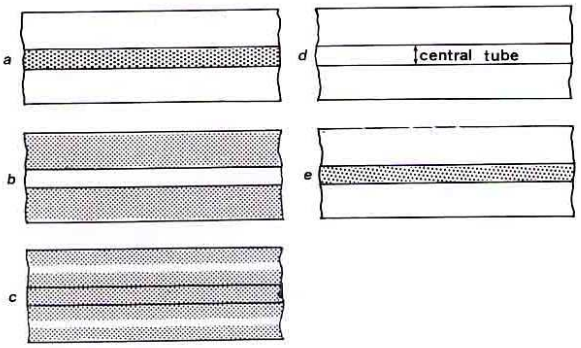

Fig. 6. Schematic representation of dark-field analysis of fig. 4.

the external parts than it is around the central core.

The cylindrical texture of the fibre can be demonstrated by dark-field analysis of the SAD pattern. Fig. 4 shows various possible positions of the aperture. The first one only intercepts the 00.2 diffracted beam. The dark-field picture becomes bright wherever aromatic layers are seen edge-on (i.e. layers parallel to the incident beam). If the texture is cylindrical, this occurs all along the fibre except right above or right below the hollow central tube (fig. 6a and 7a). The 2 posi-

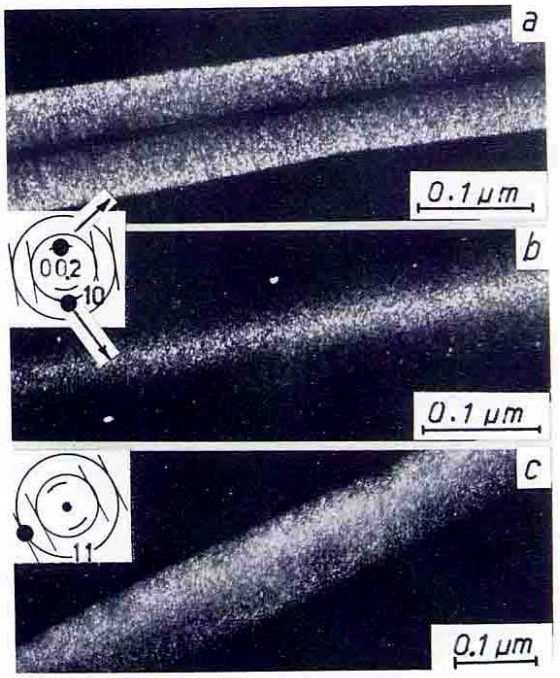

Fig. 7. Texture of a cylindrical fibre as shown by dark-field: (a) 00.2, (b) 10, (c) 11.

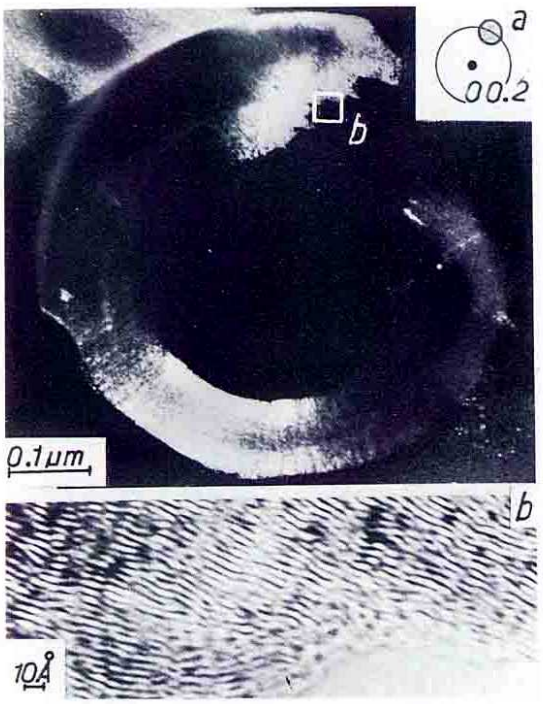

Fig. 8. Transverse thin section: (a) 00.2 dark-field, (b) 00.2 lattice-imaging of insert in (a).

tion corresponds to the reciprocal lines which are roughly parallel to the incident beam. In the optical image (figs. 6b and 7b) the central core appears as a bright band (layers seen on the upper side, i.e. normal to the incident beam). Reaching the 3 position, only the oblique reciprocal lines lead to a diffracted beam passing through the aperture. In the image (fig. 6c) the bright central band divides into two. These two bands diverge toward the edges of the fibre as the aperture moves beyond the 3 position. On the contrary, in the 4 position, if there is no preferred orientation of the *a* axis, reciprocal lines are always found which give a beam passing through the aperture. In this case, the whole fibre appears bright (fig. 6d and 7c). Finally, in the 5 position, the aperture only intercepts the beams given by the reciprocal lines normal to the incident beam. In the image (fig. 6e) the layers seen edge-on appear bright as in the 00.2-dark-field pictures.

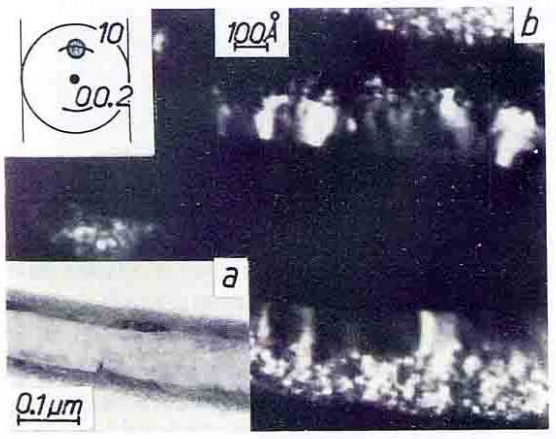

Fig. 9. Internal and external part of a fibre: (a) bright-field, (b) 00.2 dark-field.

In fig. 8a which corresponds to a transverse thin section two bright regions only appear. It has been necessary to move the aperture 180° around the 00.2 ring in order to successively light up all the other regions of the thin section.

00.2-dark-field pictures (fig. 9b) as compared to bright-field ones (fig. 9a) show two types of regions in the fibre, suggesting a different texture. The first one lying around the central tube presents intense Bragg fringes as if it were monocrystalline. Its thickness widely varies from one fibre to another. On the contrary, the second region, corresponding to outer parts of the fibres, exhibits small bright domains well separated from each other. In order to measure their sizes, is has been necessary to use an objective aperture large enough to give in the optical image plane negligible diffraction effects. Among apertures of various diameter a 0.34 $Å^{-1}$ one has been chosen which corresponds to a 3.5 Å Airy disc [the Airy disc diameter is the width at half-maximum of the central diffraction peak given by an aperture; the diameter of this aperture is expressed in the reciprocal space from the formula $(2(\sin\theta)/\lambda)$ $Å^{-1}$]. In that case, the average size of a small bright domain is less than 10 Å. These dimensions would be expected for layers of less than 10 aromatic rings piled up by 2 to 3.

The difference between the core and the external part of the fibres as well as their concentric texture are largely confirmed by two beams lattice-imaging using tilted illumination. Fig. 8b which represents an enlarged part of the transverse thin section pictured in fig. 8a, shows that the carbon layers lie parallel to the external surface of the fibre. Fig. 10a which represents a view along the fibre axis, also demonstrates the concentric texture both through the resolution of the 00.2 fringes (corresponding to the interlayer spacing seen in

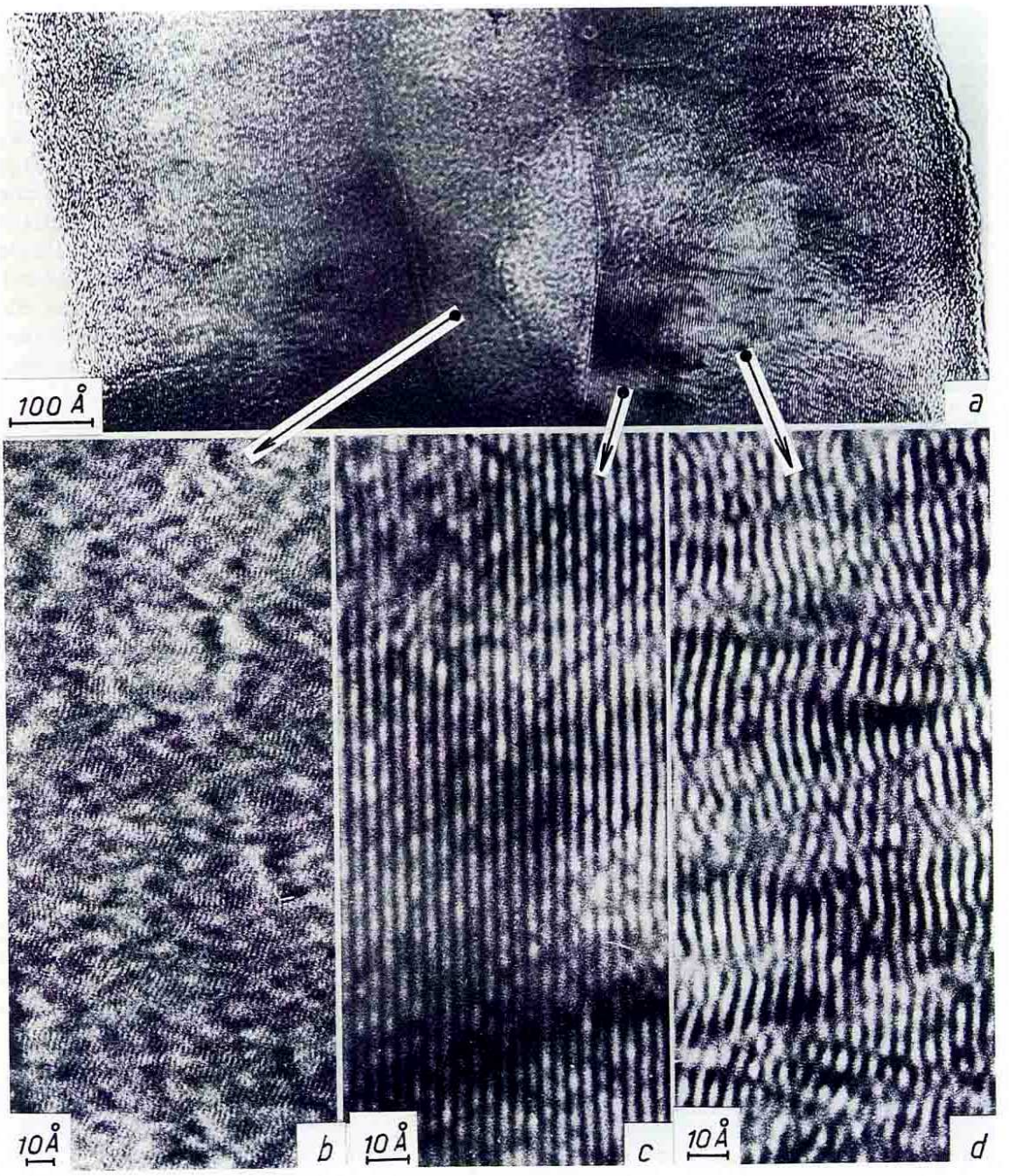

Fig. 10. Lattice-imaging: (a) view along the fibre axis, (b) 10 fringes, (c) 00.2 fringes near the hollow tube, (d) fringes in the external part

figs. 10c and 10d) and through the resolution of 10 fringes (roughly corresponding to a 2 Å periodicity seen in fig. 10b). As seen on this figure, the 10 fringes run roughly parallel to the fibre axis, in very small domains (<10 Å) separated from each other by regions out of contrast. These regions represent the portions of the fibre where 10 beams are produced which may interfere with the incident beam. This does not obviously correspond to lattice planes projection because of the turbostratic structure, but to lattice rows of

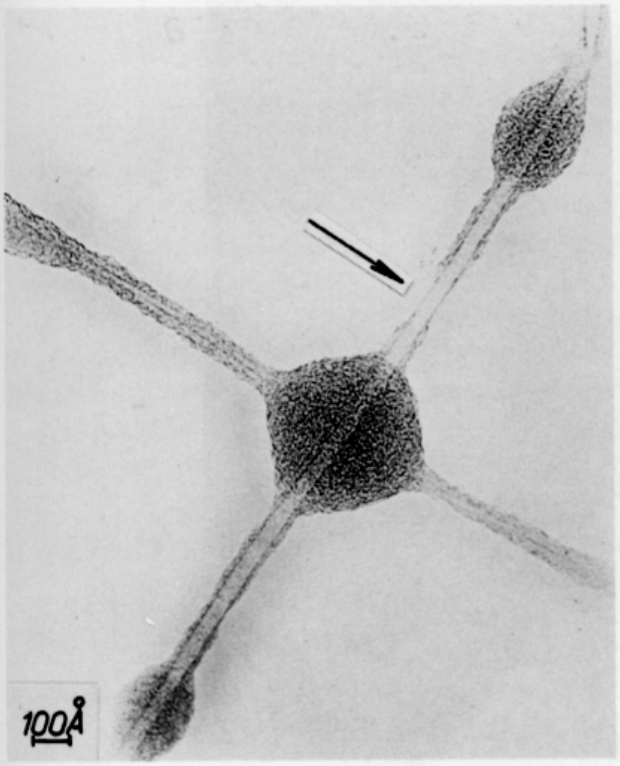

Fig. 11. Bright-field image of branched inhomogeneous fibres.

carbon atoms in a single carbon layer. Fig. 10c also shows that, near the hollow tube, the 00.2 fringes, i.e. the carbon layers, are very long, straight and perfectly parallel. The parallelism of the layers is so perfect in the vicinity of the tube that they always seem to form only one stack, thus explaining the 00.2 Bragg fringe production (which is not necessarily related to any three-dimensional order but only due to the perfect parallelism of the layers). The length of the fringes is usually more than 1000 Å. On the contrary, fig. 10d corresponding to the external part of the fibre only shows short fringes (less than 10 Å) piled up by two or three. The misorientation of one stack relatively to its neighbour ranges from 20 to 30°. This value satisfactorily agrees with the results deduced from SAD patterns. Sizes of the carbon layer stacks obtained from fringes are also in good agreement with those deduced from dark-field pictures.

The above results strongly support the occurrence of two growth processes. The first one is responsible for the formation of the inner core containing long, straight and parallel carbon layers cylindrically rolled around a hollow tube. The secondary process is the thickening of the fibre by a pyrolytic deposit. Some

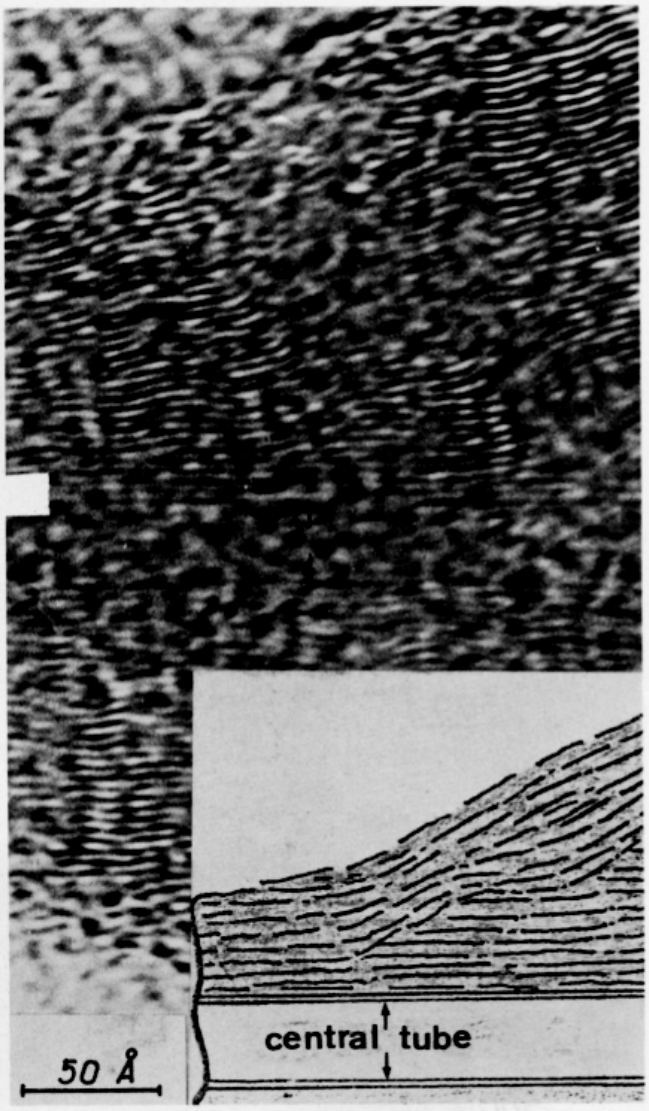

Fig. 12. (a) 00.2 lattice fringes of a constricted fibre, (b) schematic drawing of (a).

examples may be found where the internal core is only present in some part of a given fibre (see arrow in fig. 11). The same figure shows that some secondary deposit has been formed from place to place. This fact explains the conical shape of some fibres (see fig. 1c) which is probably due to an additional continuous pyrolytic deposit on an ancient one, similar to the one pictured in fig. 11. This mechanism is illustrated by lattice-imaging in the case of figs. 12a and 12b.

2.2. Tip of the fibres

Most of the fibre extremities are broken, but some of them are naturally terminated. In this latter case,

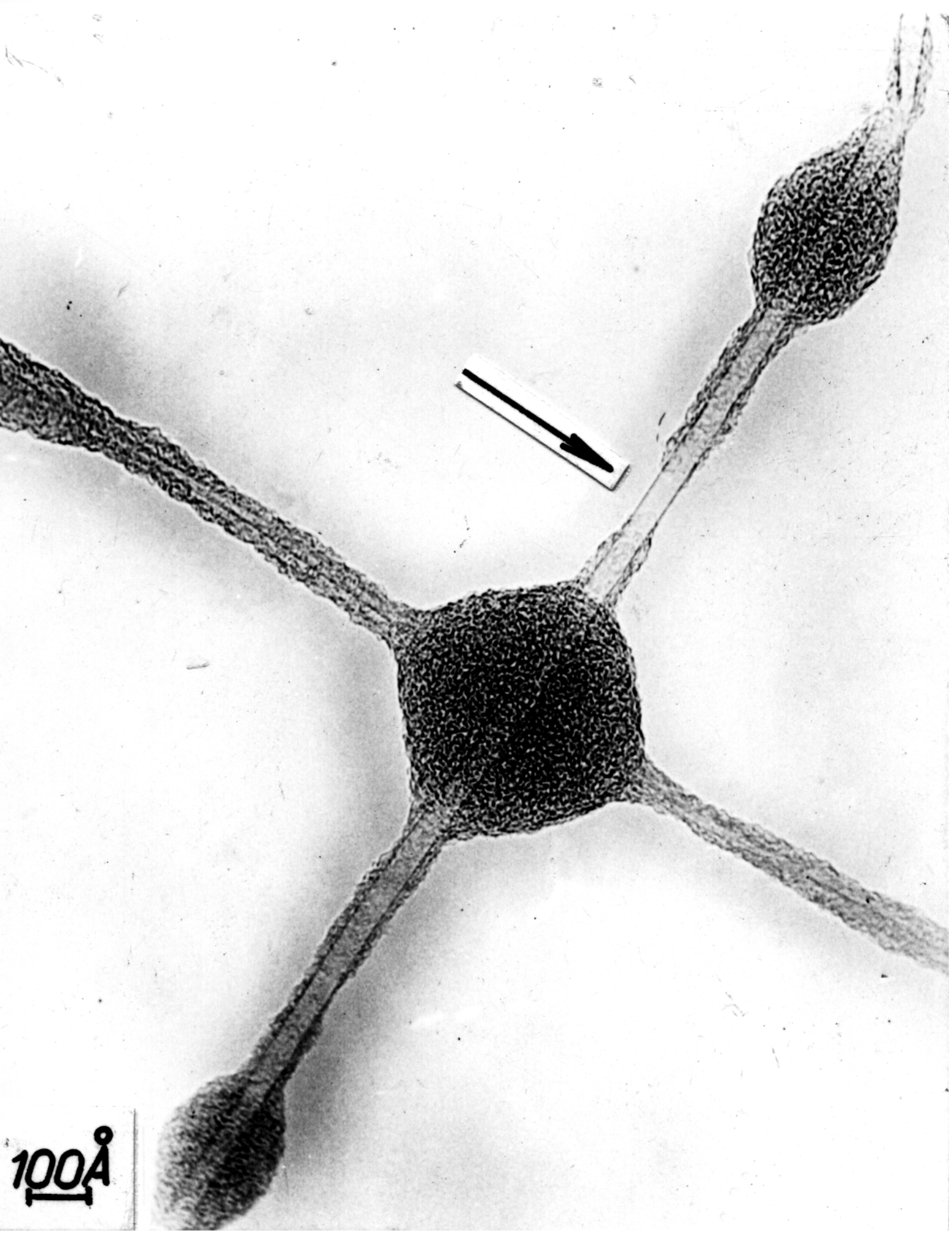
100Å

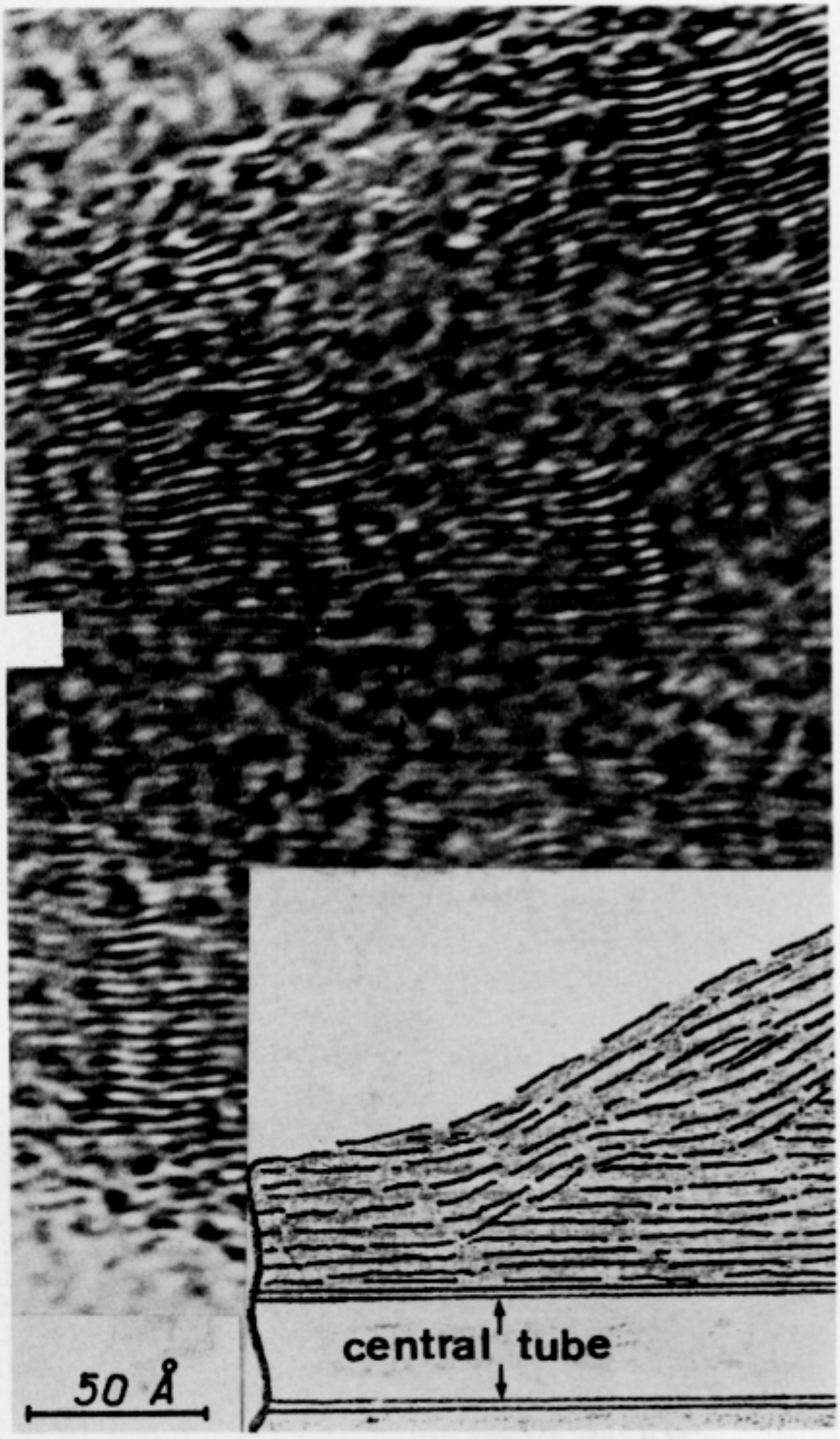

Fig. 12. (a) 00.2 lattice fringes of a constricted fibre, (b) schematic drawing of (a).

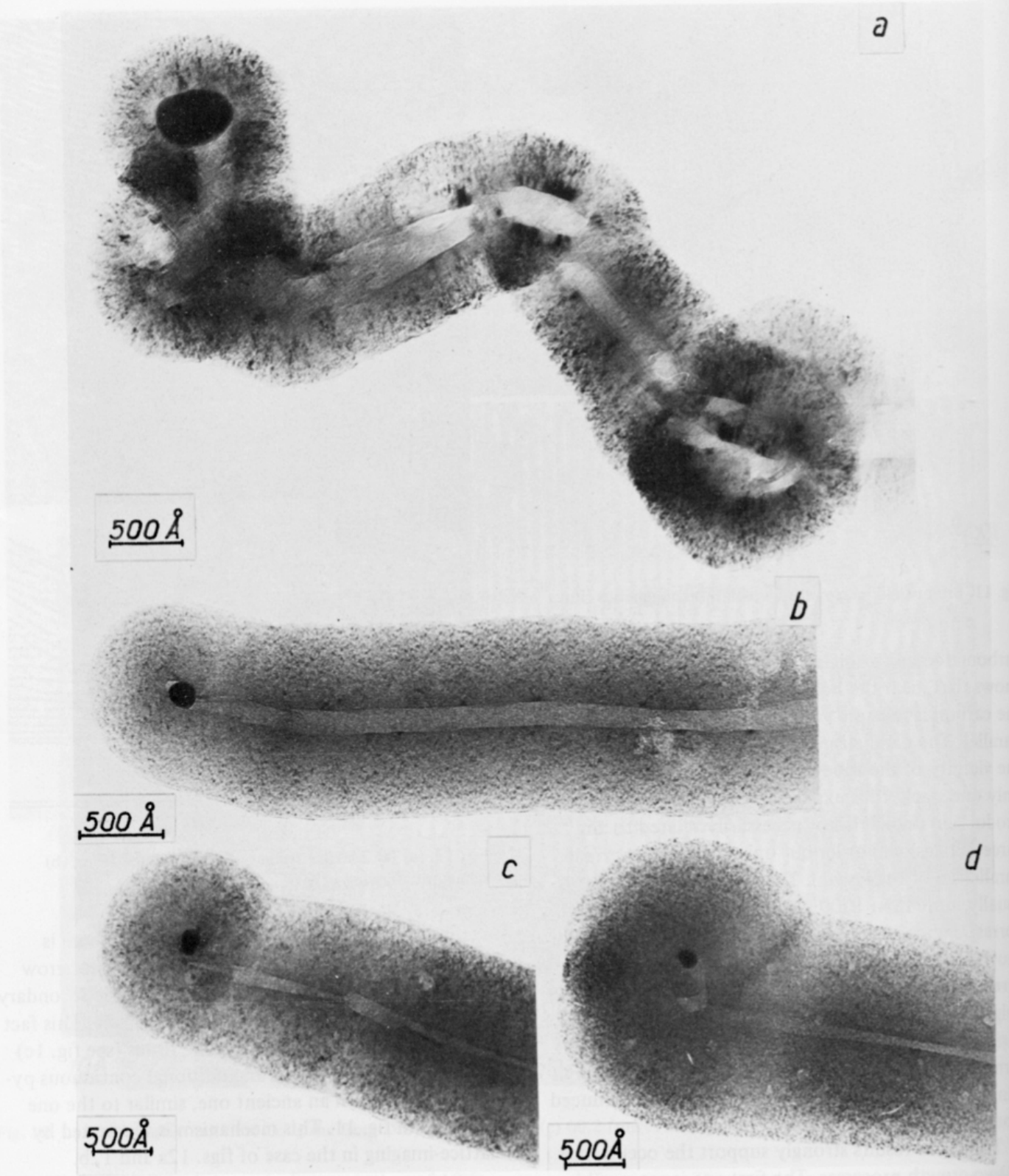

Fig. 13. Bright-field images of fibre tips showing catalyst particles.

whatever the size and shape of the fibres are, each of them contains at its tip a very small particle opaque to electrons (fig. 13). The size of these particles widely varies as it can be seen in the figure; it ranges

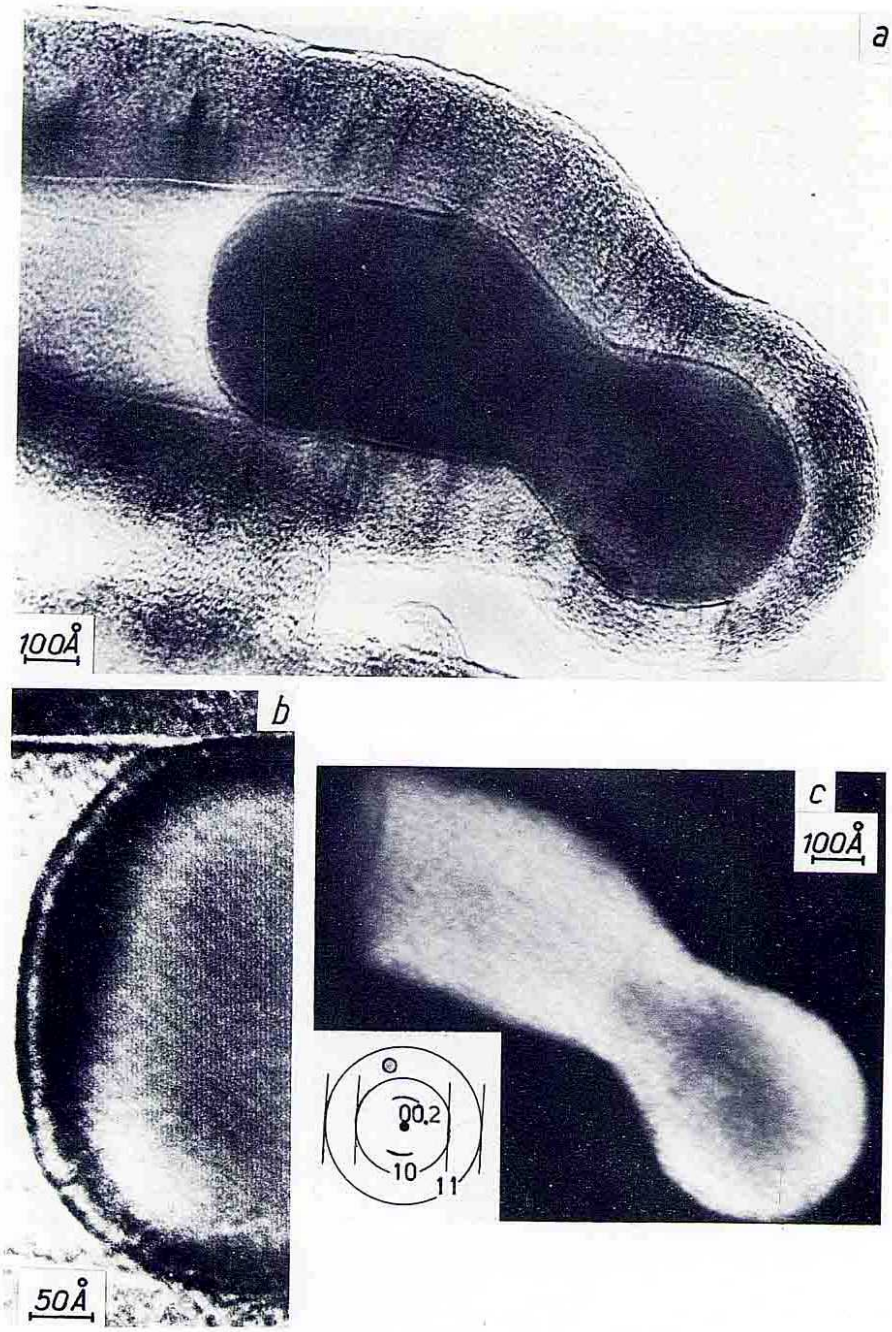

Fig. 14. Fibre tip showing FeC crystal: (a) bright-field, (b) 3.4 Å lattice fringe spacings, (c) dark-field picture with aperture centred on 210 carbide reflection (d = 1.65 Å).

from about 80 Å to 700 Å. The largest particles produce one or two very faint reflections visible in their SAD patterns. Values of d spacings thus measured suggest the possibility of either α iron or cementite Fe_3C, the most intense reflections of which being at the same place, i.e. 2.02 Å (see table 1). Lattice imag-

Table 1
X-ray powder diffraction data for Fe_3C, FeC and α-iron

Fe_3C		FeC		α-Fe	
d (Å)	*hkl*	*d* (Å)	*hkl*	*d* (Å)	*hkl*
		3.40	002		
		2.85	(102)		
		2.64	–		
		2.58			
2.54	020				
		2.50	(010)		
2.38	112, 021				
2.26	200				
2.20	120				
		2.16	110		
2.10	121				
2.06	210	2.06	111		
2.02	022			2.02	110
2.01	103				
1.97	211				
		1.93	–		
1.87	113				
1.85	122				
		1.82	202		
1.76	212				
		1.70	004		
1.68	004, 023				
		1.65	(210)		
1.61	221				
		1.56	203		
1.58	130				
				1.43	200
				1.17	211
				1.01	220

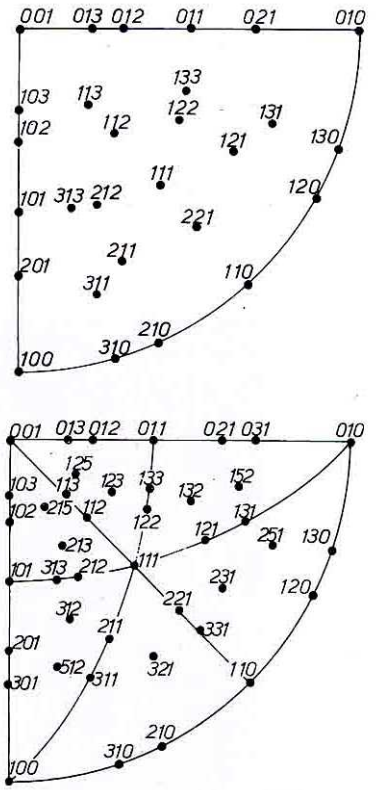

Fig. 16. Stereographic projections: (a) of Fe_3C, (b) of a cubic crystal on their (001) crystal face.

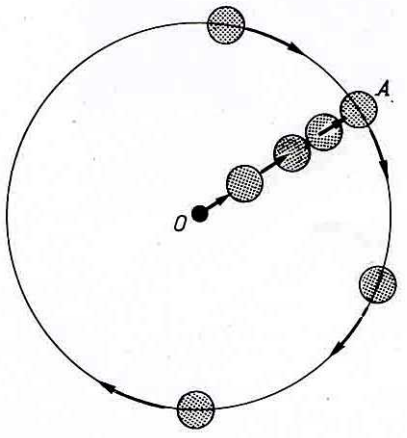

Fig. 15. Schematic representation of various positions of the objective aperture relatively to the pattern.

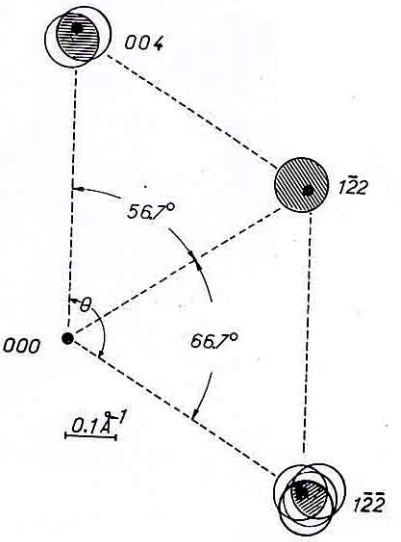

Fig. 17. Synthetic SAD pattern of small catalyst particle obtained through various objective aperture centre positions.

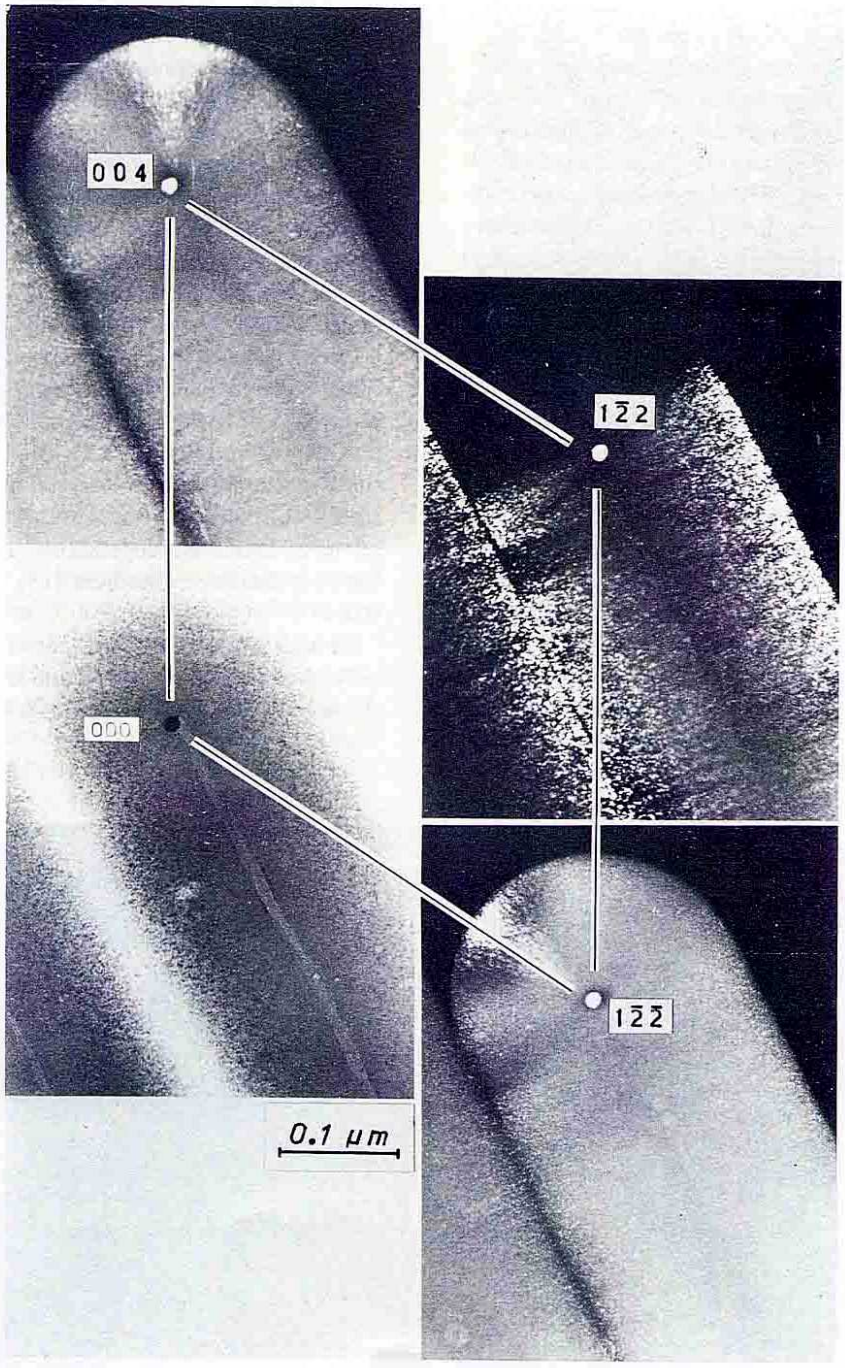

Fig. 18. Bright- and dark-field pictures of cementite crystal obtained from the fig. 17 positions of the objective aperture (the aperture also intercepts the 00.4 beam of carbon, which thus lights up).

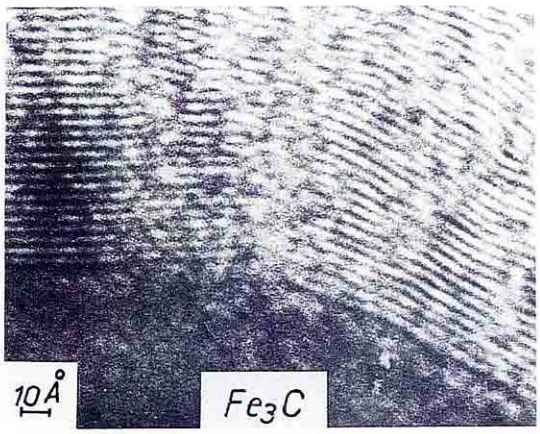

Fig. 19. Lattice-imaging of carbon encapsulating cementite crystal.

ing sometimes shows in the opaque particles, fringes with about 3.4 Å spacing eventually belonging to FeC (figs. 14a and 14b). Occurrence of iron is also suggested by spectroscopic analysis of the fibres (0.005 wt% iron content). As the smallest (and more numerous) particles are too small to give a diffraction pattern we used dark-field techniques in order to identify them.

In a previous paper, one of us has shown [13] that it is possible to measure the d spacing of a crystal as follows. A very small aperture (0.06 $Å^{-1}$) was used and the pattern was progressively tilted either radially or around a circle as indicated in fig. 15. Whenever the unknown crystal lights up very strongly in the optical image, the aperture intercepts one of its diffracted beam. Even if this latter is invisible in the SAD pattern, it can be revealed by the aperture centre position. When the crystal is lit up at its maximum, the relative position A of the aperture is pictured relatively to the unscattered beam O (fig. 15). The value of OA gives the d spacing value of the crystal if, at the same time, the $L\lambda$ constant of the apparatus is measured. Precision of the measurement depends on the aperture size and has been discussed elsewhere [13]. It is about 0.018 $Å^{-1}$.

It is known that the SAD pattern of one crystal only gives two values of d_{hkl} and the angles between the reciprocal rows, i.e. the angles between the corres-

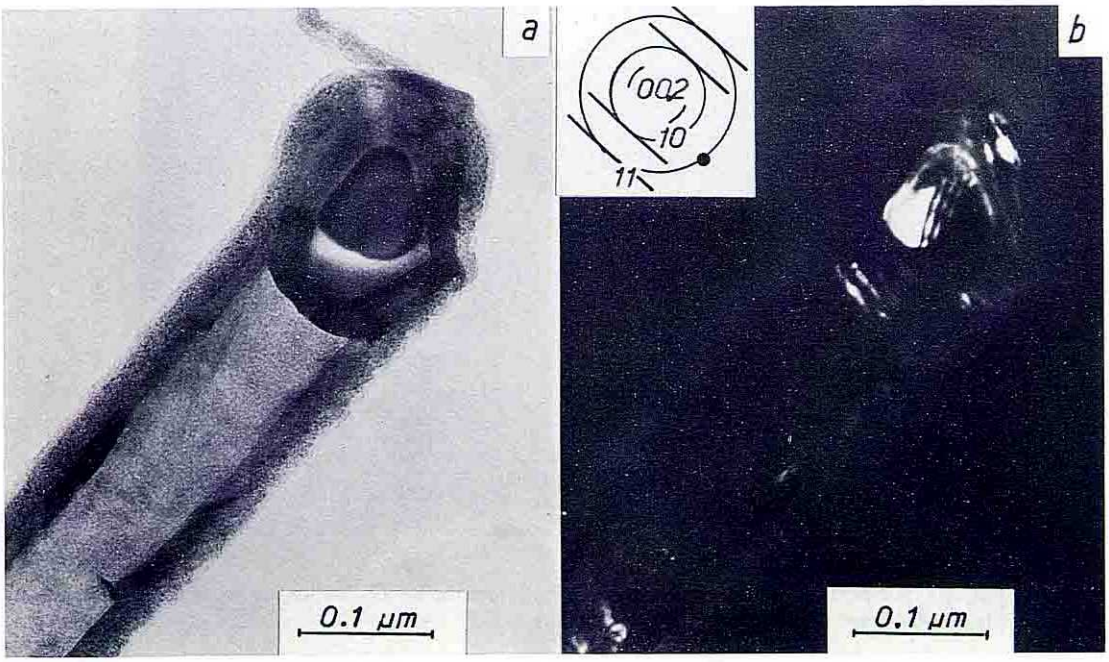

Fig. 20. Fibre tip showing relics of Fe_3C trapped within the carbon shell: (a) bright-field, (b) dark-field.

ponding planes in the crystal. Consequently, in order to identify an unknown material it is necessary to obtain more than one SAD pattern, i.e. more than one reciprocal section, and to determine the proper indices of the reflections. For that purpose, all possible crystal faces to the material have to be presented on a stereographic projection. Figs. 16a and 16b show for instance the projections for cementite and for a cubic crystal established by Andrews et al. [15]. These projections have been scaled to a Wulff pattern from which we may know all the possible angles between any reciprocal row.

Figs. 17 and 18 show an example of such a determination made on the tip of the fibre. Fig. 17 shows both the unscattered beam and every position of the objective aperture, which leads to the illumination of the small unknown particle. Some of these positions present a common part (grey areas in fig. 17). Owing to this, the location of the unknown diffracted beam becomes more precise. It may thus be deduced that the diffracted beams of the unknown particle lie on the 004 and 122 rings of cementite, and consequently do not belong to an α iron particle (see table 1). At last, the angle θ between the two reciprocal rows can be measured and its value well fits with the values calculated for Fe_3C. In fig. 18 we arranged the bright- and dark-field images in the same positions as those of the incident beam and of the diffracted beams in the synthetic SAD pattern of fig. 17. Owing to the Wulff pattern, additional information has been obtained: the indices of the crystal face which lie parallel to the supporting film; in the case of fig. 18, it is 210. The same experiments were repeated on other small particles and cementite was always found (except in the case of fig. 14c in which the position of the aperture in the pattern is compatible with FeC).

When a fibre is naturally terminated two types of carbon layer planes may occur at its tip. Sometimes the layers are long, straight and perfectly parallel to every crystalline face of the cementite crystal (fig. 19). In the other cases cementite particles are not encapsulated by a primary catalytic deposit as above, but are only covered with the secondary pyrolytic deposit. In the latter the catalytic shell narrows at its end against the carbide crystal surfaces (see fig. 14a). Relics of iron carbide layers are noticed to remain in the tip of some fibres, outside of the crystal itself but trapped in the carbon shell (fig. 20a and 20b).

3. Discussion

The above experimental results indicate that growth of thin primary fibres is due to catalytic mechanism, initiated by very small soots located in the furnace. These have been identified afterwards as iron oxide particles, reduced in pure iron by hydrogen present in the furnace. Experiments are still going on to reproduce the initial stages of growth in using small iron oxide particles.

The formation of filamentous carbon by catalytic action has been widely studied by many authors for decomposition of various kinds of hydrocarbons as well as for dismutation of carbon monoxide. Transition metals, such as iron, nickel, and cobalt, are well-known to be active catalysts, but the exact mechanism of their action is still hypothetic. Reactions are known to be favoured by presence of hydrogen, and then oxides can be used. Some authors claim that the active catalyst could be an iron carbide such as Fe_7C_3 [16], FeC [17] or Fe_3C [18]. In this case, in order to explain the hollow tube, it is necessary to assume that the carbon layers may only nucleate on a specific face of the carbide crystal. If so, a given carbide is able to solve a larger amount of poorly, than of well-organized crystalline carbon, depending on their chemical potential [18, 19]. Consequently, catalytic carbon would be produced on the active crystalline face of the carbide at the expense of the supersaturated solution of carbon contained in the carbide [20]. Such a hypothesis has the disadvantage of being based upon an hypothetic difference between the various faces of the carbide crystal. On the contrary, one of the authors [14, 21] has shown that the carbon shells resulting from carbide decomposition always present a constant thickness whatever the Miller indices of the crystal face. According to those studies, carbon layers always nucleate in a parallel direction with any available interface, only in a proportion relative to the quantity of carbon atoms provided. The interface can be either solid–gas or solid–vacuum interface [14]. Recently Baker et al. [22, 23] assume that the catalyst should be similar to a liquid droplet (which seems reasonable according to the temperature range and the size of the droplets [24, 25]). They also assume that the reaction of decomposition of the hydrocarbon, which occurs on the available portion of the droplet, is exothermic and creates a temperature gradient along the diameter of

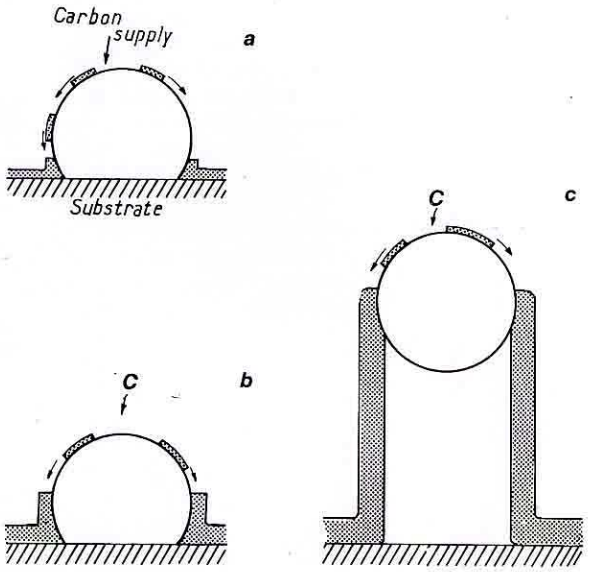

Fig. 21. Schematic illustration of fibre growth through catalytic effect.

the droplet. The carbon thus tends to nucleate on the side portions of the drop unprotected from carbon deposition because of their contact with the furnace. All these interpretations consider the diffusion of carbon atoms either through the metal or through the carbide and do not take into account any possible diffusion of metal into carbon. Moreover all of them do not really satisfactorily explain anisotropy of the growth and the occurrence of a central hollow tube.

An explanation which seems more satisfactory has been proposed by Baird et al. [26] involving a surface diffusion of "metal–metal hydrocarbon species" across the edge of the carbon layer planes. At the beginning small "liquid-like" droplets of iron get fixed on the wall of the furnace, resulting from the reduction by hydrogen of iron oxide soots. On that clean surface begins to nucleate an association of metal and hydrocarbons which diffuses on the surface and dissociates at the contact angle between the droplet and the wall of the furnace acting as a substrate. The beginning of a carbon shell is then produced. New metal hydrocarbon species dissociate on its edges and the carbon layers develop by lateral growth following the external surface of the catalyst (figs. 21a and 21b). Such a lateral growth exerts a force strong enough to lift up the catalyst particle above the surface of the substrate (fig. 21c). Layers always progress laterally in the same way and result in a filament. The hollow channel in the centre is due to the fact that no carbon supply can reach the back of the droplet, the surface of which is protected from downward surface migration by the lateral carbon layers. Growth of carbon layers would continue as long as there is a supply of metal from the top of the catalyst particle (the metal being progressively trapped between the carbon layers). When the whole droplet is covered by carbon layers at the tip, the diffusion stops and growth ends. This kind of mechanism is strongly supported by the existing relics of cementite found inside the carbon shell (see fig. 20). It must be noticed that cementite crystals are obviously formed only when cooling occurs. Such a mechanism also well explains branching of the fibres.

Increase in thickness by pyrolytic deposit on the primary thin fibres is a common phenomenon leading to graphitizable carbon. The constricted aspects often encountered at that stage of growth are probably due to the temperature gradient created along the fibre axis by a catalyst particle existing in that place. This may also be due to fluctuations of the gas flow in the reaction furnace. Anyway, such a deposit is similar to pyrolytic carbon, i.e. it is strongly oriented with its carbon layers approximately parallel to the substrate; but it is made of small turbostratic stacks with tilt and twist boundaries and thus looks more defective than the catalytic carbon contained in the core.

References

[1] W.R. Davis, R.J. Slawson and C.R. Rigby, Nature 171 (1953) 756.
[2] L.J.E. Hoffer, E. Stering and J.T. MacCartney, J. Phys. Chem. 59 (1955) 1153.
[3] L. Meyer, Z. Krist. 109 (1957) 61.
[4] M. Hillert and N. Lange, Z. Krist. 111 (1958) 24.
[5] R. Bacon, J. Appl. Phys. 31 (1960) 283.
[6] M.L. Lieberman, C.H. Hills and C.J. Miglionico, Carbon 9 (1971) 633.
[7] F.E. Wawner, Jr., J. Appl. Phys. 44 (1973) 502.
[8] T. Koyama, M. Endo and Y. Onuma, Japan. J. Appl. Phys. 11 (1972) 445.
[9] T. Koyama and M. Endo, Oyo Buturi 42 (1973) 690.
[10] T. Koyama and M. Endo, Japan. J. Appl. Phys. 13 (1974) 1175.
[11] T. Koyama, M. Endo and Y. Hishiyama, Japan. J. Appl. Phys. 13 (1974) 1933.
[12] A. Oberlin and G. Terrière, J. Microscopie 14 (1972) 1.

[13] A. Oberlin, G. Terrière and J.L. Boulmier, J. Microscopie 21 (1974) 301.
[14] A. Oberlin, G. Terrière and J.L. Boulmier, Tanso (Japan) 80 (1975) 29; 84 (1975) 16.
[15] K.W. Andrews, D.J. Dyson and S.R. Keown, in: Interpretation of Electron Diffraction Patterns (Hilger and Watts, London, 1967) p. 164.
[16] W.R. Ruston, M. Warzee, J. Hennaut and J. Waty, Carbon 7 (1969) 47.
[17] A. Oberlin and J.P. Rouchy, Carbon 9 (1971) 39.
[18] H.P. Boehm, Carbon 11 (1973) 583.
[19] J. Gillot, B. Lux, P. Cornuault and F. du Chaffaut, Ber. Deut. Keram. Ges. 45 (1968) 224.
[20] E. Fitzer and B. Kegel, Carbon 6 (1968) 433.
[21] J R. Comte-Trotet, Thesis, to be published.
[22] R.T.K. Baker, M.A. Barber, P.S. Harris, F.S. Feates and and R.J. Waite J. Catalysis 26 (1972) 51.
[23] R.T.K. Baker, P.S. Harris and R.B. Thomas, in. Proc. Intern. Congr. Carbon, Baden-Baden, 1972, p. 91.
[24] J.J. Métois, Thesis, Marseille (1974).
[25] K.L. Chopra, Thin Film Phenomena (McGraw-Hill, New York, 1969).
[26] T. Baird, J.R. Fryer and B. Grant, Carbon 12 (1974) 591.